ELSEVIER

Polymer 41 (2000) 7209–7221

polymer

Molecular dynamics simulation study of norbornene–POSS polymers

R.K. Bharadwaj[a], R.J. Berry[b], B.L. Farmer[b,*]

[a]*Systran Federal Corporation, Dayton, OH 45431-1672, USA*
[b]*Air Force Research Laboratory, Materials and Manufacturing Directorate, AFRL/MLBP WPAFB, OH 45433-7750, USA*

Received 15 September 1999; received in revised form 7 December 1999; accepted 22 December 1999

Abstract

Atomistic molecular dynamics simulations have been used to delineate the effects of introducing polyhedral oligomeric silsesquioxane (POSS) moieties substituted by cyclopentyl and cyclohexyl rings as pendant groups on polynorbornene. Simulations were also performed on polynorbornene for comparison. Calculated volume–temperature behavior and X-ray scattering profiles matched well with experimental results. Most importantly, the effects of incorporating the POSS moieties into the polymer have been identified via simulations. These were judged on the basis of the increase in the glass transition temperature, retardation of the chain dynamics and improvements in the calculated elastic tensile, bulk and shear moduli of the POSS containing polymers compared to the norbornene homopolymer. The most important conclusion from the study is that aggregation of the POSS moieties is not required for the beneficial effects to be realized. Indeed, the simulations show that there is no tendency for aggregation to occur among the POSS moieties if they are well dispersed to begin with over the time scale of the simulation. Packing features are delineated with the aid of intermolecular site–site radial distribution functions. In addition, the mean squared displacement of the POSS moieties in the polymer matrix was found to be very small at all temperatures leading to a slowing of the segmental dynamics of the polymer chain, and thereby imparting the macroscopically observed stiffness. It is reasoned that the chief source of reinforcement arises from the POSS moieties behaving as strong anchor points in the polymeric matrix. This has more to do with the ponderous nature of these moieties versus any specific intermolecular interactions.

Keywords: Polyhedral oligomeric silsesquioxane; Polynorbornene; Molecular dynamics simulations

1. Introduction

An appealing goal in polymer science and technology involves the development of polymeric materials reinforced on the spatial scale of a few nanometers. One route to developing such materials has been through the incorporation of inorganic groups such as POSS (polyhedral oligomeric silsesquioxane) into conventional organic polymer matrices [1]. This is done by introducing them either as pendant groups or as part of the polymer backbone. POSS moieties are essentially polyhedral cages composed of Si and O atoms with the chemical formula Si_8O_{12}. The Si corner atoms are usually connected to organic groups such as cyclopentyl or cyclohexyl rings. Such inorganic–organic hybrid polymers possess several attractive properties such as increased thermal stability, higher glass transition temperatures, better flame and heat resistance and enhancements in the modulus and melt strengths [2]. Importantly, these property enhancements occur at low POSS contents ($<$10 mol%). POSS chemistry is very flexible [1,3]. A wide variety of substituents may be affixed on the Si atoms at the corners of the cages to optimize polymer–POSS interactions and simultaneously to aid in the easy dissolution of the POSS moieties in common solvents for synthesis purposes. These groups may be incorporated into almost any conventional polymer and in a variety of different chain architectures. POSS moieties have been incorporated as pendant groups in polynorbornene [4], poly(4-methylstyrene) [5,6], polymethacrylate [7] and ethene–propene [8] copolymers, as part of the main chain in siloxane [9,10] polymers and epoxies [11], as cores in dendrimers [12] and in highly porous POSS based network polymers [13].

Though the effects of incorporating the POSS moieties into polymeric matrices are well known as described above, the precise nature and the origin of this reinforcing behavior is still a matter of debate. The goal of the present work is to achieve an understanding of the structure–property relationships extant in these organic–inorganic hybrid polymers using atomistic molecular dynamics (MD) simulations. In particular, the origin of the reinforcing effects of the POSS moieties and the nature of

* Corresponding author. Tel.: + 1-937-255-9209; fax: + 1-937-255-9157.
E-mail address: barry.farmer@afrl.af.mil (B.L. Farmer).

0032-3861/00/$ - see front matter
PII: S0032-3861(00)00072-0

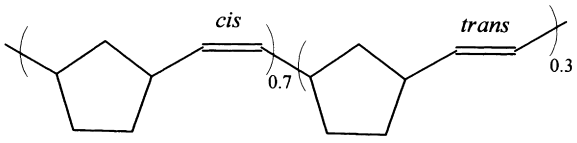

Poly(norbornene) (PN)

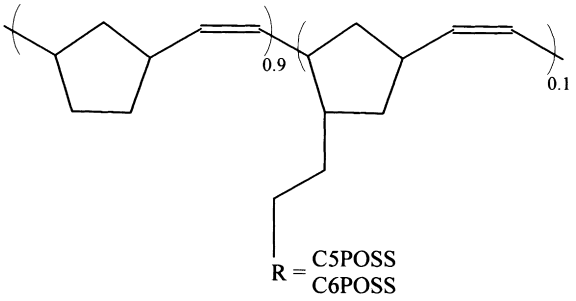

Poly(norbornene-*ran*-norbornene-POSS) copolymers (C5PN and C6PN)

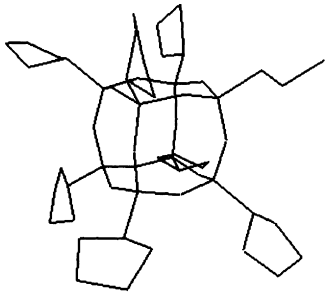

C5POSS

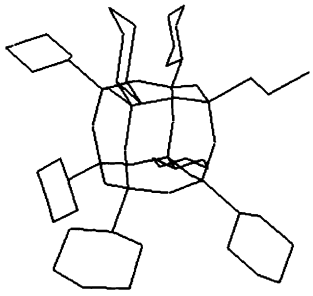

C6POSS

Fig. 1. Repeat unit structures of the simulated polymers. All three polymers (PN, C5PN and C6PN) were built with a *cis* content of 70%. The cyclohexyl (C6POSS) and cyclopentyl (C5POSS) substituted polyhedral oligomeric silsesquioxane (POSS) moieties are also shown. The central cage is composed of Si (at the corners) and O (along the edges). The cyclopentyl and cyclohexyl rings are connected to the corner Si atoms.

POSS–polymer interactions are the main subjects of the study. Towards this end we have chosen the POSS–norbornene polymeric system which has been the subject of previous experimental investigation. For the purposes here the precise system of choice is not very crucial since the effects of incorporating POSS into a polymer is largely independent of the polymeric matrix involved. While the extent of reinforcement or enhancement of properties is a function of the polymeric matrix, the underlying mechanisms governing the POSS–polymer interactions are similar in all cases. By bringing atomistic MD simulations to bear on this system, we hope to delineate the interactions directly at the spatial scale at which they occur.

2. Simulation details

2.1. Systems studied

The systems studied consisted of ring opening polymerized norbornene homopolymer (PN) and its random copolymers with norbornene–POSS (POSS moiety connected to the norbornene monomer by an ethyl spacer) and are depicted in Fig. 1. Two different types of POSS moieties were considered. In one case the cyclopentyl rings (C5POSS) were attached to corner Si atoms and in the other case cyclohexyl rings (C6POSS) were attached. In all there were seven rings per POSS moiety with the eighth Si corner atom attached to the ethyl spacer connecting it to

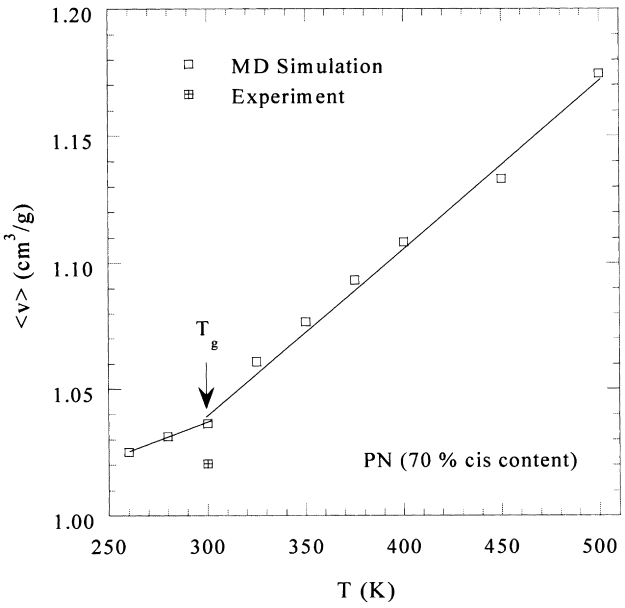

Fig. 2. Specific volume vs. temperature for PN at 0 atm as determined from NPT dynamics (open squares, thin curve). Experimental data [23,24] for PN at 300 K is also shown. The arrow locates the position of the MD determined T_g.

the norbornene unit. In the simulations, the copolymers were built by including 10 mol% of the norbornene–POSS monomer with 90 mol% of norbornene. These copolymers are named C5PN and C6PN depending on the type of POSS moiety used as a pendant group (C5POSS vs. C6POSS). Alternatively, the copolymers could be visualized as a polynorbornene chain with C5POSS or C6POSS pendant groups grafted by means of an ethyl spacer at random locations on the main chain. The presence of an unsaturated linkage in the PN backbone leads to two configurations *cis* and *trans* that can be formed at the unsaturated bond. A *cis* content of 70% was chosen in order to facilitate comparison both within the simulation generated results for the three polymers as well as with experimental results [4]. The polymers were built as single chains consisting of 100 monomeric units each. In the case of the random copolymers, 10 units of the appropriate co-monomer were introduced into the chain. This corresponds to a POSS content of 10 mol% (approximately 50 wt%). There were 1702, 2932, and 3142 atoms per chain for the PN, C5PN and C6PN systems, respectively.

2.2. Molecular dynamics details

All simulations were performed using the *Discover*® program employing the *Compass*® forcefield [14]. The single polymer chain was packed into a large cubic simulation cell at a low density ($\sim$0.3 g cm^{-3}) and subsequently densified by performing MD simulations under *NPT* (constant particle number, pressure and temperature) conditions at 0 atm and 500 K. The resulting box sizes of the well equilibrated configurations were 26.38, 31.96 and 32.57 Å for PN, C5PN and C6PN, respectively. Temperature and pressure were controlled by using the Andersen [15] and Berendsen [16] methods, respectively. The velocity [17] form of the Verlet [18] integrator was used to integrate the equations of motion with a time step of 1 fs. *NPT* dynamics were used to study the three polymers over a temperature range of 260–500 K. Electrostatic interactions were dealt with by the distance dependent dielectric constant method [19] using a dielectric constant of 2.5. Long range corrections [20] to the system energy and pressure were explicitly taken into account. A cutoff radius of 10.0 Å was used in all simulations. Computations were carried out on a Silicon Graphics ORIGIN multiprocessor machine using between four and eight processors.

For all three polymeric systems the simulations were initially conducted at 500 K for more than 1 ns duration to obtain well-equilibrated samples. Systems at lower temperatures were created from this sample by cooling in 50 K intervals until 400 and 30 K intervals for temperatures lower than 400 K. The simulations were run for 500 ps for all temperatures other than 500 K for the three systems. Specific volumes achieved equilibration after 100–200 ps, depending on the temperature.

3. Results and discussion

3.1. Volume–temperature behavior

The computation of the volume–temperature (V–T) properties via MD simulations serves two important purposes. First, it facilitates comparison with experimental data and therefore forms an excellent basis for judging the quality of the force field parameters used in the simulations and directly measures the ability of the simulation to mimic the real polymeric systems. Second, it allows the prediction of one of the most important material properties of a polymer, the glass transition temperature (T_g) [21,22]. This is achieved in much the same fashion as is done experimentally where the specific volume is measured at different temperatures at constant pressure. A break in the slope of the V–T curve represents the location of the T_g. In simulations, the specific volumes are predicted as a function of temperature at a given pressure via *NPT* dynamics. The time averaged specific volumes are presented as a function of temperature in Fig. 2 for PN and Fig. 3 for C5PN and C6PN systems. In all three cases, breaks in the slopes of the V–T curves indicative of vitrification are found. The arrows mark the location of the MD determined T_g.

The V–T properties for the three polymers are summarized in Table 1. There is little in the way of experimental V–T data for the three polymers except for T_g values determined from Differential Scanning Calorimetry (DSC) experiments. In the case of PN there exists experimental data [23,24] for the specific volume at room temperature as given in Table 1. It has been experimentally observed

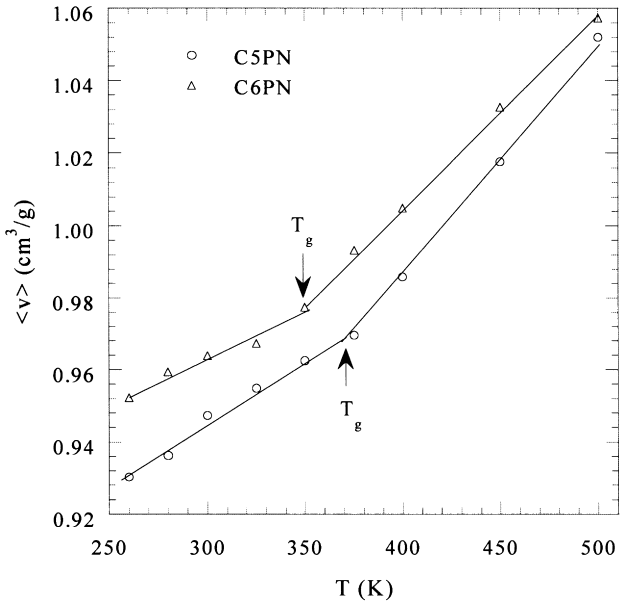

Fig. 3. Specific volume vs. temperature for C5PN (open circles and thin curve) and C6PN (open triangles and thin curve) at 0 atm as determined from NPT dynamics. The arrows locate the breakpoints indicating the position of the MD determined T_g. Both had 10 mol% of the appropriate POSS moiety (C5POSS or C6POSS).

that the density of the PN homopolymer is unaffected by the stereoregularity of the chain. The difference between the experimental and simulation result at 300 K is very small, with the simulation predicting slightly lower density (by 2%) compared to experiment. The glass transition temperature from simulations is located around 300 K. This compares favorably with experimental values for the T_g of 304 [23] and 325.3 K [4] at a *cis* content of 60% and 316 K [24] for the PN homopolymer with 70% *cis* content. As mentioned previously, all three polymers were constructed with *cis* content of 70% at the unsaturated linkage. The densities of the polymers follow the order C5PN > C6PN > PN over the entire temperature range. We note also from Fig. 3 that the *V–T* curve for C6PN is shifted to higher values than C5PN. The lower density obtained for C6PN is direct evidence that cyclohexyl substituted POSS results in poorer packing efficiency compared to cyclopentyl substituted POSS. It may therefore be deduced that the packing environment in C5PN is a little different from that in C6PN. This will be explored in greater detail in the following section.

The most important observation from the *V–T* results presented in Figs. 2 and 3 and summarized in Table 1 is that the incorporation of C5POSS and C6POSS moieties as pendant groups on the PN main chain *increases* the T_g with respect to the PN homopolymer. This is in excellent agreement with experimental observations [4] that show T_g increases with incorporation of POSS moieties onto polymeric chains regardless of the type of polymer. In the simulations, the C5PN and C6PN copolymers contained 10.0 mol% of the appropriate POSS co-monomer (C5POSS or C6POSS). The experimental data for the T_g for polymeric systems with slightly lower POSS content [4] (8.4 mol% for C5PN and 7.7 mol% for C6PN) are also given in Table 1. The general agreement of the simulation predicted T_g values with experiment is good in both cases. However, the T_g of C5PN predicted from simulations is *higher* compared to that for C6PN at the same POSS content. This is contrary to experimental results where PN containing C6POSS pendant groups has a higher T_g compared to that containing C5POSS pendants.

The origin of this discrepancy is difficult to pinpoint for several reasons. First, in the case of poly(4-methylstyrene) [5,6] containing C5POSS pendant groups, the T_g is found to be higher than that for the polymer with C6POSS pendant groups. Experimentally, the T_g was found to be 409 vs. 395 K at 8 mol% of C5POSS and C6POSS pendant groups on poly(4-methylstyrene), respectively. This has been found to be true at several different concentrations of POSS and is especially evident at higher POSS contents. Therefore, incorporation of C5POSS can indeed lead to higher T_g compared to C6POSS at the same concentration in the polymer. Also, the difference in the T_g values of poly(4-methylstyrene) with C5POSS and C6POSS pendant groups is negligible at low POSS contents (<10.0 mol%). Second,

Table 1
Volume–temperature properties for PN, C5PN and C6PN at atmospheric pressure

Polymer	$\langle v \rangle$ (MD)[a] $cm^3\ g^{-1}$	$\langle v \rangle$ (exp)[a] $cm^3\ g^{-1}$	T_g (MD) K	T_g (exp)[b] K	α (MD)[c] $10^{-4}\ K^{-1}$	δ (MD)[d] $(MPa)^{1/2}$
PN	1.036	1.02[e,f]	300	304[e], 316[f], 325.3[g]	5.64	15.2
C5PN	0.947	–	370	342[h]	6.49	12.0
C6PN	0.964	–	350	354[i]	5.20	11.3

[a] Specific volumes at 300 K.
[b] T_g from DSC measurements.
[c] Volumetric thermal expansion coefficient in the melt region.
[d] Solubility parameter at 300 K.
[e] From Ref. [23] (60% *cis* content).
[f] From Ref. [24] (70% *cis* content).
[g] From Ref. [4] (60% *cis* content).
[h] From Ref. [4], 8.4 mol% of cyclopentyl POSS (71% *cis* content).

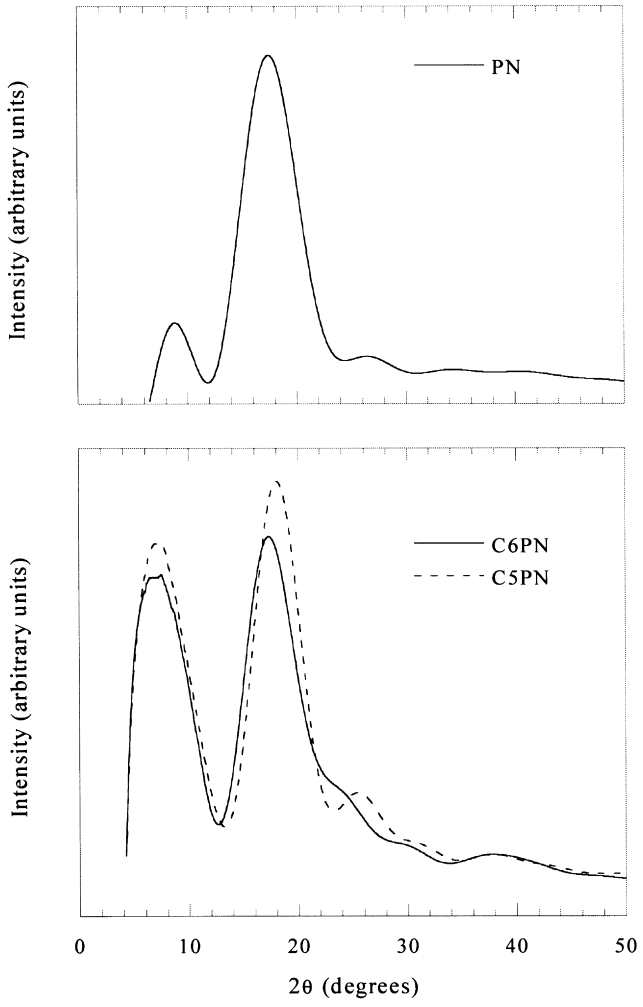

Fig. 4. X-ray scattering intensity (powder pattern, Cu-Kα) vs. scattering angle for PN (top), C5PN and C6PN (bottom) at 300 K obtained from simulation.

in the case of C5PN and C6PN, we note that the experimental results [4] are at slightly lower concentrations of the POSS compounds 8.4 and 7.7 mol%, respectively, compared to simulation, which is at 10 mol%. Although, the difference in concentration between experiment and simulation is only on the order of 2 mol% it should be recognised that this may correspond to a rather large effect on the properties due on the large physical size of the POSS moieties. Last, to determine the T_g from simulations, fairly long trajectories (on the order of a few nanoseconds duration) would be required for greater confidence in the results [21,22]. The *V-T* results in this study were generated by simulation runs on the order of 0.5 ns owing to computational constrains. The cause for the above discrepancy could be rooted in the simulation methodology adopted here, but perhaps more reasonably, further simulations as well as experiments on different polymeric matrices containing C5POSS and C6POSS pendant groups at different concentrations would be needed to resolve the issue satisfactorily.

The volumetric coefficient of thermal expansion is approximately the same for C6PN and PN polymers with that for C5PN being slightly higher as seen from Table 1. In addition, the solubility parameter (δ) has been calculated from simulations at 300 K and are presented in Table 1. The sum of the intermolecular dispersion and electrostatic interactions was taken to be the cohesive energy. In a system simulated with periodic boundary conditions, a polymer chain will have many images. The non-bonded (dispersion and electrostatic) intermolecular energy is that between the parent chain and its images [25]. Interactions occurring between atoms on the same chain segment in the central simulation cell separated by distances that are smaller than the cutoff radius constitute intramolecular interactions. Therefore, all interactions may be classified into either of the intra or intermolecular types. In the computation of the solubility parameter only the intermolecular part of the interaction energy is used. The correction to the system energy due to the use of a cutoff (tail correction) is also explicitly included in the intermolecular energy. Normalization of the cohesive energy with molar volume yields the cohesive energy density. The solubility parameter is obtained by taking the square root of the cohesive energy density. No direct experimental data are available for the solubility parameters of these three polymers. From simulation, the solubility parameter is lower for C5PN and C6PN than for the PN homopolymer. In addition, δ for C5PN is slightly higher than that for C6PN. Strictly on the basis of chemical composition, the difference between C5PN and C6PN is negligible; therefore the difference in δ can be ascribed to the differences in packing in the two polymers. As noted earlier, the density of C6PN is lower compared to that for C5PN indicating less efficient packing. In consequence, the interaction energy between the POSS moieties and the surrounding polymer is also reduced, leading to an overall reduction in the solubility parameter. The packing aspects (where much of the cause for the above behavior resides) is taken up next.

3.2. X-ray scattering profiles

It is of interest to understand the structure of the polymer in the presence of POSS moieties. In addition, experimental [4] X-ray scattering intensity profiles for the three polymers allow for comparison. The X-ray scattering intensities were computed from the simulations at 300 K for PN, C5PN and C6PN and are shown in Fig. 4. A broad amorphous halo may be discerned at 2θ values of 17.5, 18.1 and 17.2° for PN, C5PN and C6PN, respectively. These correspond to *d*-spacings of 5.2, 4.9 and 5.1 Å. This peak is attributed to the scattering from the C and H atoms in the PN backbone and therefore occurs at approximately the same 2θ value in all three polymers as expected. This is in excellent agreement with experimental results ([4, Fig. 11(i) and (vi)]) which show the peak at 2θ of ~18.2 (*d*-spacing 4.9 Å) in all three polymers. Upon incorporation of the POSS moieties, a second amorphous halo appears at 2θ of ~7.2°

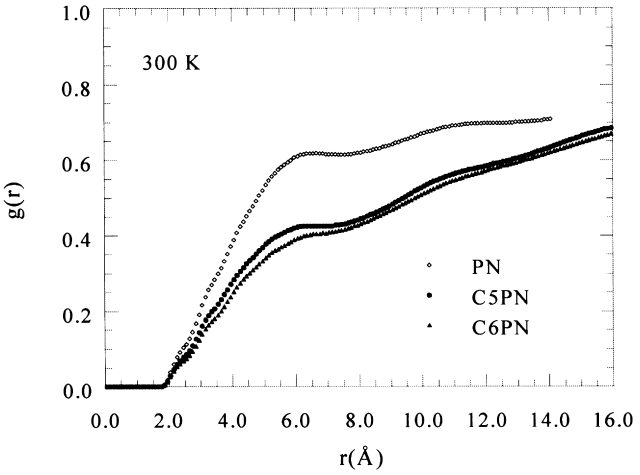

Fig. 5. Intermolecular radial distribution functions based on all atom centers for PN, C5PN and C6PN at 300 K.

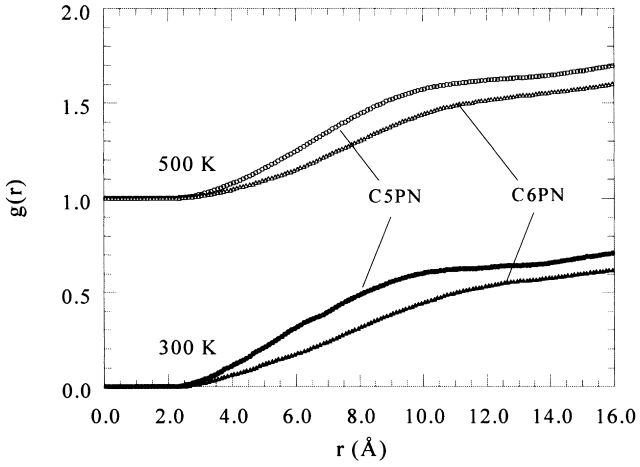

Fig. 6. Site–site intermolecular radial distribution function based on cyclopentyl and cyclohexyl POSS moieties (Si, O, C, and H atom types) to the main chain (C, H atom types) for C5PN and C6PN at 300 and 500 K. The curves for 500 K have been shifted for clarity.

(*d*-spacing ~12.3 Å) in the simulation predicted scattering profiles for C5PN and C6PN. This represents the scattering from the C5POSS and C6POSS moieties. This peak (2θ ~7.2°) is approximately of the same intensity as the peak at 2θ ~18.0°. From experiments this peak is located at approximately 2θ ~7.6° (*d*-spacing 11.7 Å) and increases in intensity with increasing POSS content. Experimentally [4], for the C5PN case, an additional peak appears as a shoulder on the 2θ ~7.2° peak at high C5POSS contents (>5.0 mol%). Evidently, this peak is not observed in the simulations. We also note the presence of a low intensity peak in the PN case at a 2θ of 8.9° (*d*-spacing ~9.9 Å) suggesting the presence of some degree of long range ordering in this case as well. This peak was not observed in the only available experimental pattern [4] for PN. The several other features in all three patterns at higher 2θ values originate chiefly from the intramolecular structure of the polymer chains.

3.3. Radial distribution functions

The radial distribution function $g(r)$ and various site–site distribution functions provide a more intimate understanding of the packing details. The intermolecular $g(r)$ based on all atom centers in the systems is shown in Fig. 5. In all three cases (PN, C5PN and C6PN) there is a diffuse peak at ~6.0 Å. The position is shifted to slightly larger distance for C6PN. This essentially represents the average interchain spacing. However, we note that the $g(r)$ behavior is different for the three polymers in its dependence on the radial distance. The $g(r)$ for PN has a higher value at any given distance compared to those for C5PN and C6PN. This implies that although the interchain spacing of the chains is largely unaffected by the presence of the POSS moieties, the number of such interchain contacts in a given volume is decreased due to their presence. Furthermore the $g(r)$ for C5PN is slightly higher than that for C6PN indicating that the number of intermolecular contacts is higher per unit volume for C5PN. The following physical picture emerges from this analysis. The packing between the PN chains of the backbone is essentially the same in all three cases but in the case of C5PN and C6PN, the PN chains are separated by the POSS moieties. The presence of 10 mol% of the POSS units translates to approximately 50 wt%. That is, the POSS units occupy approximately half the volume of the system. Therefore although the interchain packing is the same in the polymer surrounding the POSS units, the number of such contacts is greatly reduced over a given volume element. This effectively leads to the depletion in the $g(r)$ for the POSS containing polymers. We also note the presence of several shoulders on the curves in the region 2.0–4.0 Å. These features are probably due to H–H intermolecular contacts. At still larger distances (over 10.0–12.0 Å), a very diffuse overtone may be seen in Fig. 5 for all three cases.

The intermolecular packing of the backbone polymer chain around the POSS units has been shown in Fig. 6 at 300 and 500 K. This site–site radial distribution function was constructed by considering all the atoms in the POSS units with all the atoms in the PN backbone. A very diffuse peak is seen in the region 10.0–12.0 Å for C5PN whereas the $g(r)$ for C6PN is essentially featureless. This indicates that the packing of chains around C5POSS is more structured than the very diffuse packing around C6POSS. In addition, the $g(r)$ has a higher value at any given r for C5PN compared to C6PN. This indicates that the density of the PN–POSS contacts is higher in the case of C5PN. The behavior evidenced here is a manifestation of the intrinsic conformational and structural attributes of the C5POSS and C6POSS moieties. In particular the behavior is related to the packing of the substituents around the polyhedral cage. The geometry of the polyhedral cage composed of Si and O atoms is a highly constrained one although capable of

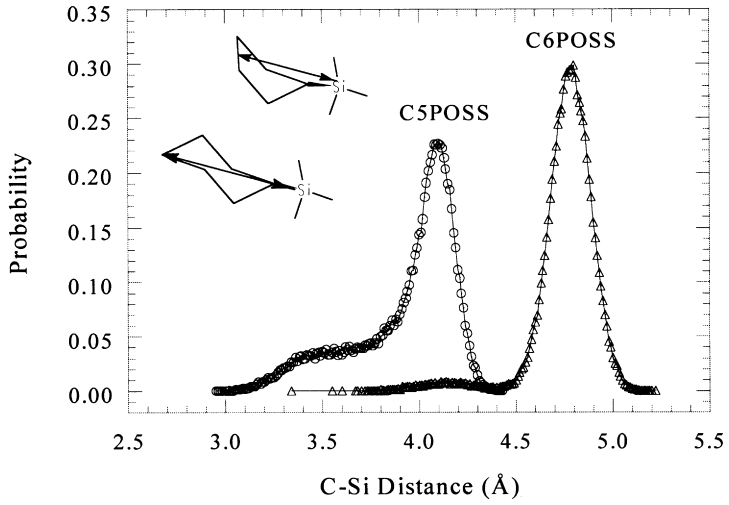

Fig. 7. Probability distribution for the distance between the Si atom of the cage and the farthest C atom of the ring attached to it at 500 K. For clarity, the definition of the distances is shown in the schematic (inset). In the cyclopentyl case, the distance is from the midpoint of the C–C bond to the Si atom as shown.

small deformations. The body diagonal of the polyhedra (Si–Si distance) in both cases was distributed around 5.4 Å. Therefore the only difference is in the manner in which the cyclopentyl or cyclohexyl rings pack around the POSS polyhedra. To better understand this difference, the distances of the C atom on a ring located the farthest from the Si atom to which it was connected was monitored during the simulations at 500 K. This is shown more clearly via the schematic representation inset in Fig. 7. This distance was averaged over all such contacts in the system. This measures the extent to which the rings are spread out with reference to the polyhedral cage. The distribution of these distances is shown for C5POSS and C6POSS in Fig. 7. In case of the cyclopentyl ring the distance is smaller than for the cyclohexyl ring by almost 1.0 Å. Cyclopentyl units can approach the polyhedra (the cage composed of Si and O atoms) closer and therefore are packed more compactly and thereby allow the polymeric chains to approach closer. In addition, the small size of the rings allows for rotations/inversions to take place and facilitate packing. In the cyclohexyl case, the presence of the sixth methylene unit drastically alters the conformational space. Serious steric hindrances prohibit efficient packing around the POSS polyhedra as evidenced from the data presented in Fig. 7. The rings were found to adopt the chair conformation predominantly and fanned out from the central cage although a small population of the boat conformer may also be discerned (in the r region 3.5–4 Å of Fig. 7). This result is contrary to the situation in neat cyclohexane where the boat–chair ring inversions are ubiquitous. The presence of the sixth methylene unit precludes the assumption of the boat conformation facing towards the polyhedron due to the serious steric repulsion between the sixth methylene unit and the oxygen atom of the POSS cage (which occurs at three equivalent positions 120° apart). Therefore the boat conformation can exist only when the boat is formed such that the sixth methylene unit is pointing away from the POSS cage.

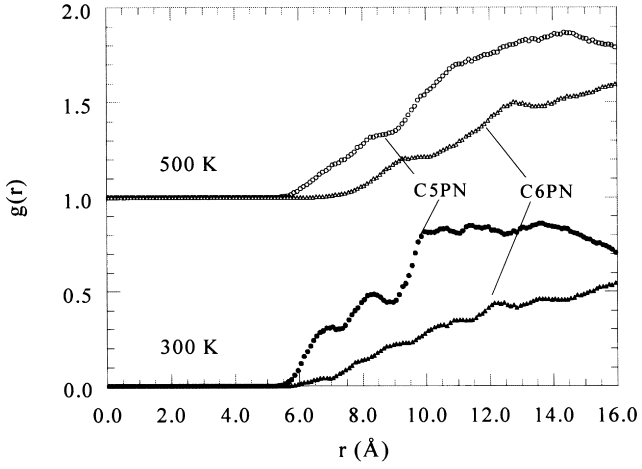

Fig. 8. Site–site intermolecular radial distribution function based on POSS moiety to POSS moiety (Si and O atom types) for C5PN and C6PN at 300 and 500 K. The curves for 500 K have been shifted for clarity.

There is great interest in how the POSS moieties assemble in polymeric matrices with respect to one another. We address this by constructing the site–site intermolecular $g(r)$ based on the Si and O atoms of every POSS molecule in the system. This is shown in Fig. 8 at 300 and 500 K. In general the packing for the C5POSS case is more efficient compared to that for C6POSS. This is directly related to the difference in physical size of these two moieties as discussed above. The curves at 500 K are smoother compared to those at 300 K indicating some mobility of the POSS polyhedra. At lower temperature, the polyhedra remain stationary and therefore the $g(r)$ behavior is more structured. The $g(r)$ data indicate that there is no tendency for the POSS units to aggregate. This was also confirmed via visual inspection of several snapshots of the systems where the POSS moieties were uniformly distributed in the simulation cell.

Any close contact between the POSS moieties was only a consequence of being tethered to the main chain at a very short distance apart. The fact that there is no tendency for aggregation of the POSS moieties to occur within the time frame of the simulations and assuming no aggregation to begin with is an important one. This essentially means that proximity is only a function of where the POSS moieties occur along the chain, which is a random occurrence. At high POSS loadings physical proximity is a natural outcome due to the bulky nature of these moieties and should not be confused with aggregation, which indicates a tendency for POSS moieties to self-associate. Most importantly, the effects of the POSS moieties on the polymers here are due entirely to the presence of POSS and not to any aggregation effects, which have often been suggested to explain various experimental observations.

3.4. Mobility of the silsesquioxane polyhedra

The mean square displacement (MSD) of the POSS polyhedra in C5PN and C6PN was computed from the following expression:

$$\mathrm{MSD} = \langle |r_i(0) - r_i(t)|^2 \rangle \tag{1}$$

where r represents the coordinates of atom i. This analysis yields information about the diffusive characteristics of the POSS moieties. The brackets denote the averaging achieved by considering multiple origins (1 ps apart) along the original simulation trajectory as starting points, and also, averaging over all POSS moieties in the system. The MSD is shown in Fig. 9 for the C5POSS and C6POSS polyhedra at several different temperatures. The behavior is mostly associated with localized motion of the POSS moieties. That is, the POSS moieties are confined to a cage formed by the surrounding polymer chains and perform non-diffusive motions within this cage. This is seen to be true regardless of the temperature in case of C6POSS moieties where the MSD is found to be no more than 3.0 Å^2 over a duration of 400 ps. In the case of C5POSS however, the onset of diffusive behavior is seen to emerge at 450 and 500 K. At 400 K and lower temperatures the behavior is non-diffusive identical to that seen in C6POSS. This contrasting behavior of the C5POSS and C6POSS moieties may be rationalized based on the compact structure of C5POSS, which lead to higher MSDs compared to C6POSS as discussed in the previous section. It is therefore proposed that the reinforcement effects arise from the fact that the POSS moieties remain stationary over a wide temperature range and act as strong anchoring points in the polymeric matrix.

3.5. Conformational dynamics

Although a very detailed study of the conformational properties is outside the purview of the present work, it is appropriate to address some aspects of the conformational

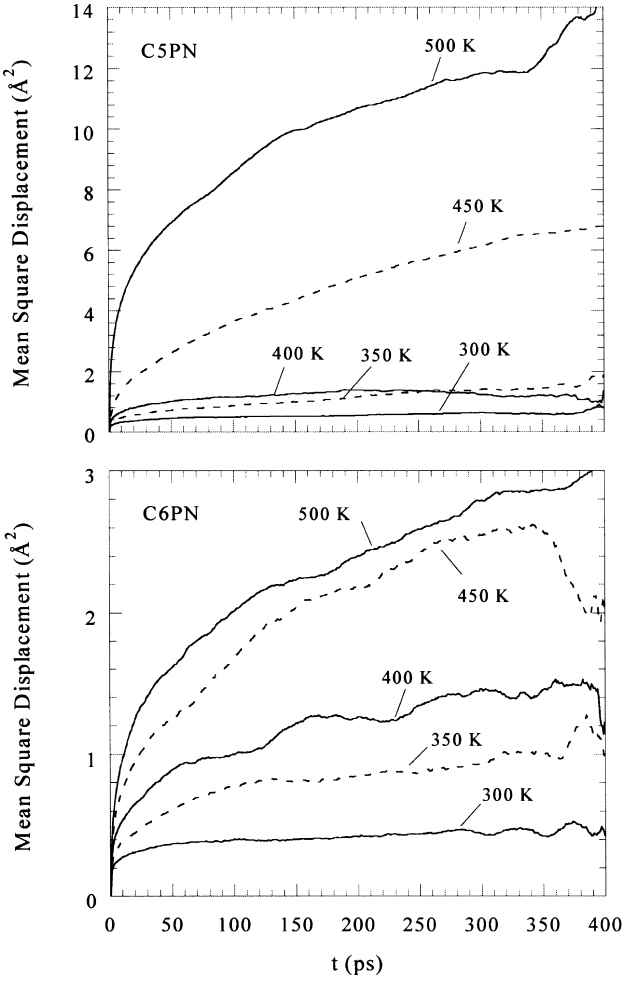

Fig. 9. Mean square displacements of the POSS moieties at different temperatures in C5PN (top) and C6PN (bottom). The trajectories have been averaged over all 10 POSS moieties in the system. The mean square displacement was computed based on the center of mass of the POSS polyhedra consisting of Si and O atoms. The difference in scale on the vertical axis is to be noted.

dynamics in these polymers. The effect of incorporation of the POSS moieties as pendant groups on the conformational dynamics was probed by computing the torsional autocorrelation function (TACF) [26] given by

$$f_\phi(t) = \frac{(\langle \cos\phi(0)\cos\phi(t)\rangle - \langle\cos\phi(0)\rangle^2)}{(\langle\cos\phi(0)^2\rangle - \langle\cos\phi(0)\rangle^2)} \tag{2}$$

where ϕ represents the value of the torsional angle and the brackets denote ensemble averaging over the torsions in the system. The practice of initiating the calculation of the ACFs from multiple origins (50 ps apart) in the original simulation trajectory was employed to yield an averaged ACF. The TACFs were fit by the Kohlrausch–Williams–Watts (KWW) [27–29] stretched exponential given by

$$f(t) = \mathrm{e}^{-(t/\tau)^\beta} \tag{3}$$

where τ represents the relaxation time and β the width of

Table 2
Kohlrausch–Williams–Watts parameters for various TACFs at 500 K

Polymer	Main chain TACF		Ring-POSS TACF		Ethyl spacer TACF	
	τ (ps)	β	τ (ps)	β	τ (ps)	β
PN	3.65	0.26	–	–	–	–
C5PN	7.15	0.21	9.54	0.38	281.37	0.55
C6PN	12.25	0.17	18.26	0.37	1627.70	0.31

the process. The TACFs were constructed for several different torsional types in the system. The resulting KWW parameters (τ and β) are given in Table 2 for TACFs based on different torsional angles.

We address the influence of the POSS moieties on the main chain relaxation first. For this the main chain torsions as defined in the inset in Fig. 10 were considered. The TACF based on all main chain torsions in the system for all three polymers is shown in Fig. 10 at 500 K. The curves represent KWW fits to the simulation data. Most importantly, the main chain relaxation in C5PN and C6PN is slower compared to PN. Also the relaxation associated with C5PN is faster than C6PN. It is therefore concluded that the main chain relaxation is very sensitive not only to the presence but also the type of POSS moiety attached to it.

It is of interest to probe the relaxation behavior of the cyclopentyl and cyclohexyl substituents on the POSS polyhedra. The TACF based on the torsional angle of the ring–POSS linkage is shown in Fig. 11. Here again the TACF decay has been fit by the KWW stretched exponential. We find that cyclopentyl rings relax faster than cyclohexyl rings. This supports the view that the cyclopentyl group is relatively unobtrusive compared to the cyclohexyl group. Its small size allows more freedom for torsional motion about the ring–POSS bond.

Lastly, we report the TACFs based on the ethyl spacer torsion that connects the POSS moieties to the main chain. The relaxation associated with this is shown in Fig. 12 where it is seen that the relaxation associated with this motion is extremely sluggish compared to the main chain relaxation and the relaxation of the rings. In keeping with the behavior seen above, the relaxation of the spacers connecting the C6POSS units to the main chain is slower than that of the spacers connecting C5POSS. This slow relaxation is to be expected since the conformational freedom of the spacer is drastically reduced since its rearrangements can occur only through highly cooperative motions of the main chain and the bulky POSS moieties.

An aside is appropriate at this point regarding the anomalous T_g behavior noted earlier. The T_g in the case of C5PN was found to be higher compared to C6PN from the V–T results (Section 3.1). From the above conformational analysis it is clear that the chain dynamics in the case of C6PN is slower compared to C5PN regardless of the type of relaxation monitored. Based on the slower main chain dynamics in C6PN compared to C5PN it would be reasonable to expect a higher T_g for C6PN compared to C5PN. At present, we are unable to explain this anomaly. However, it has been demonstrated beyond doubt in this work that the presence of even isolated POSS moieties has a profound impact on both local (ring–POSS, ethyl spacer) and global (main chain) relaxation behavior.

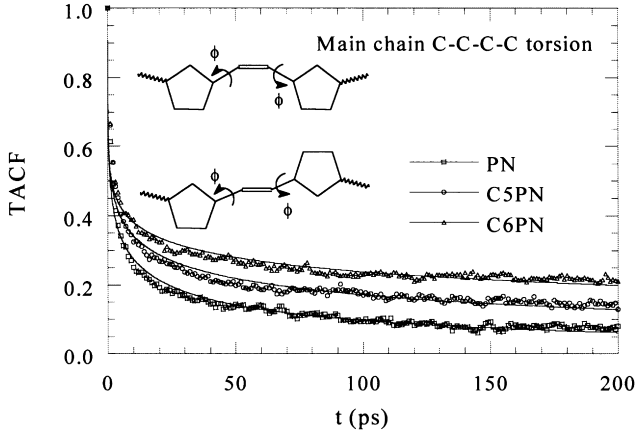

Fig. 10. Main chain segmental relaxation at 500 K in PN, C5PN and C6PN. The definition of the torsional angle used in constructing the torsional angle autocorrelation function (TACF) is as depicted in the schematic (inset). The curves correspond to KWW fits to the MD data (points).

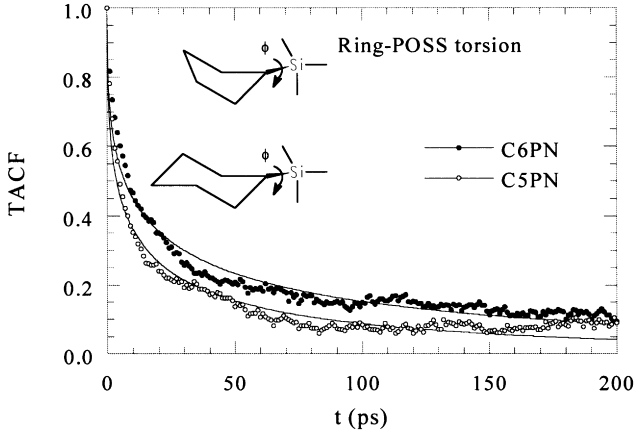

Fig. 11. Decay of the torsional autocorrelation function for the ring–POSS torsion at 500 K. The definition of the torsional angle is as depicted in the schematic (inset). The curves correspond to KWW fits to the MD data (points).

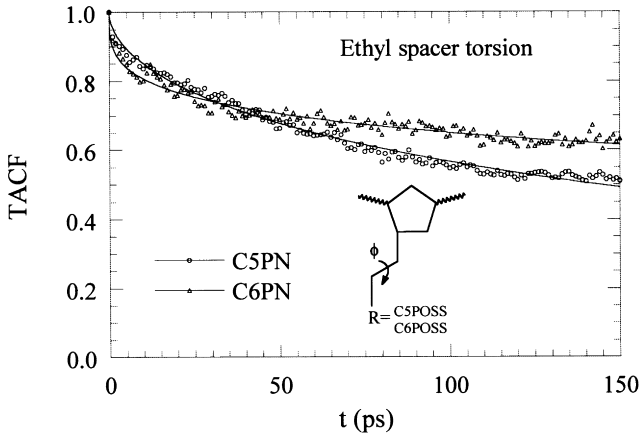

Fig. 12. Decay of the torsional autocorrelation function associated with the ethyl spacer connecting the POSS moiety to the main chain at 500 K. The definition of the torsional angle is as depicted in the schematic (inset). The curves correspond to KWW fits to the MD data (points).

3.6. Mechanical properties

One of the most appealing outcomes of incorporating POSS moieties onto a polymeric backbone is the enhancement of mechanical properties such as the tensile modulus. Stiffening of the polymer matrix is to be expected based on the higher T_g, and the slowing of the conformational dynamics in the presence of anchor-like POSS moieties. Therefore the computation of the mechanical properties from simulation forms an important test of its predictive abilities in designing future POSS based polymers and helps in further reinforcing the deductions from the previous analyses. From the theory of linear elasticity, the stress σ_{ij} and strain ϵ_{kl} tensors are related through the elastic stiffness tensor C_{ijkl} by [30]

$$\sigma_{ij} = C_{ijkl}\epsilon_{kl}. \tag{4}$$

Parinello and Rahman [31] recognized the fact that the fluctuations in the elastic strain provides a direct measure of the elastic constants as

$$C_{ijkl} = \frac{kT}{\langle V\rangle}\langle \epsilon_{ij}\epsilon_{kl}\rangle^{-1} \tag{5}$$

where C_{ijkl} is the elastic stiffness matrix, K the Boltzmann constant, T the temperature and $\langle V\rangle$ the average volume of the simulation cell. The convergence of this strain–strain correlation function is extremely slow and therefore a modification of this function with improved convergence properties was suggested by Gusev and coworkers [32–34] given by

$$C_{ijkl} = \langle \epsilon_{kl}\sigma_{mn}\rangle\langle \epsilon_{mn}\epsilon_{kl}\rangle^{-1}. \tag{6}$$

The convergence of this stress–strain correlation function is extremely rapid when compared to the original PR fluctuation formula (Eq. (5)). The strain tensor is computed from

$$\epsilon_{ij} = \tfrac{1}{2}\langle \mathbf{h}_{nl}\langle \mathbf{h}\rangle_{lj}^{-1}\mathbf{h}_{np}\langle \mathbf{h}\rangle_{pi}^{-1} - \delta_{ij}\rangle \tag{7}$$

where **h** represents the scaling matrix of the cell vectors **a**, **b** and **c** and δ_{ij} is the Kronecker tensor. The desired elastic constants can be obtained from constant stress simulations [35] where the cell is allowed to change both shape and size by calculating the mean squared strain and stress fluctuation expressed in terms of the instantaneous scaling matrix **h**.

In practice, the constant stress simulations [35] ($N\sigma T$) in which the cell vectors are allowed to adjust independently in response to an applied pressure were initiated from equilibrated configurations resulting from the isotropic cell fluctuation *NPT* dynamics at 300, 400 and 500 K for the three polymers. The $N\sigma T$ simulations were carried out over a period of 300 ps. Although the shape of the cell deviated from orthogonality of the initial cubic shape, the average specific volume resulting from these simulations was very close to that found from the isotropic *NPT* dynamics. A period of 100 ps was allowed to elapse before computing the C_{ijkl} matrices using Eq. (6). The various components of the stress–strain correlation achieved convergence within the 200 ps sampling time. The time averaged elastic constant matrices for the three polymers are given in Table 3. The upper limit uncertainties in the calculated values of the elastic constants are approximately 10%. We note that the elastic constant matrices at 300 K show some evidence of residual stress in the systems. This temperature is below that of the glass transition temperature for the three polymers. The presence of residual stresses in a glass is not surprising since the glassy state of a polymer is a non-equilibrium state. The situation is further exacerbated by the extremely slow chain dynamics in the glass and the very short time scales accessible to simulation in comparison. In addition, finite size of the sample accessible in simulations could also contribute to such a behavior. However, the matrices at the two higher temperatures of 400 and 500 K approach that of an isotropic material within the limits of the error involved in the calculation. Clearly, further determinations of the elastic constant matrices using the above method from simulations involving different polymeric matrices are required to gain a better understanding. Therefore, the above caveats need to be borne in mind while scrutinizing the data presented. The effective isotropic elastic constants are shown in Table 4 as a function of temperature. The reinforcing effect of the POSS moieties is clearly seen from the increase in the values of the tensile modulus in the C5PN and C6PN cases compared to the PN homopolymer. More importantly the drop in tensile modulus in the copolymer case (C5PN and C6PN) with temperature is slower than for the PN homopolymer. Furthermore, C6PN has a higher modulus than C5PN at all temperatures. This may be understood by the preceding analyses of the MSD, as well as the conformational dynamics for the C6POSS and C5POSS units. It was found that the MSD for C6POSS was smaller than that of C5POSS at all temperatures. This lack of mobility of the POSS units leads to the conclusion that the reinforcement effect arises primarily due to the POSS units behaving as strong anchoring points. In the case of C5PN, the

Table 3
Elastic constant matrices (C_{ijkl}) for PN, C5PN and C6PN (in GPa)

	300 K	400 K	500 K
PN	$\begin{pmatrix} 2.49 & 1.76 & 1.85 & -0.01 & 0.18 & 0.67 \\ 2.76 & 4.52 & 2.48 & -0.01 & 0.54 & 0.61 \\ 2.68 & 2.52 & 3.01 & 0.12 & 0.92 & 0.58 \\ 0.46 & 1.05 & 0.58 & 0.32 & -0.32 & -0.13 \\ -0.64 & -0.80 & -0.56 & -0.27 & 0.34 & -0.39 \\ 0.05 & -0.36 & -0.30 & 0.23 & 0.02 & 0.51 \end{pmatrix}$	$\begin{pmatrix} 2.42 & 1.84 & 1.89 & 0.13 & 0.01 & 0.13 \\ 0.79 & 40.98 & 0.56 & 0.07 & -0.14 & 0.08 \\ 1.79 & 1.71 & 1.47 & 0.02 & -0.17 & 0.13 \\ -0.13 & -0.07 & -0.24 & 0.21 & 0.03 & -0.07 \\ 0.02 & -0.11 & -0.11 & -0.05 & 0.20 & -0.04 \\ 0.17 & 0.10 & 0.03 & -0.01 & 0.03 & 0.21 \end{pmatrix}$	$\begin{pmatrix} 1.24 & 1.16 & 1.11 & 0.08 & -0.09 & 0.00 \\ 0.81 & 1.12 & 1.11 & 0.16 & -0.12 & 0.04 \\ 0.95 & 1.22 & 1.27 & 0.02 & -0.10 & -0.01 \\ -0.07 & -0.12 & -0.08 & 0.14 & 0.04 & -0.06 \\ -0.16 & -0.03 & -0.09 & -0.04 & 0.18 & -0.03 \\ 0.06 & 0.00 & -0.15 & 0.01 & -0.02 & 0.01 \end{pmatrix}$
C5PN	$\begin{pmatrix} 3.27 & 2.48 & 1.88 & 0.80 & -0.19 & -0.42 \\ 1.84 & 3.12 & 1.60 & 0.49 & 0.05 & -0.04 \\ 2.32 & 2.99 & 3.51 & 0.57 & 0.15 & -0.08 \\ 0.59 & 0.71 & 0.45 & 0.44 & -0.08 & -0.22 \\ -0.59 & -0.46 & -0.36 & 0.16 & 0.64 & -0.21 \\ -0.32 & -0.04 & 0.09 & 0.00 & -0.52 & 0.46 \end{pmatrix}$	$\begin{pmatrix} 2.14 & 0.89 & 0.34 & -0.15 & 0.14 & 0.07 \\ 2.43 & 2.87 & 1.41 & -0.29 & 0.06 & 0.13 \\ 1.87 & 1.49 & 0.62 & -0.15 & 0.22 & -0.11 \\ 0.09 & 0.03 & 0.09 & 0.51 & -0.11 & -0.02 \\ 0.00 & -0.16 & -0.06 & 0.10 & 0.43 & -0.16 \\ 0.10 & 0.14 & 0.02 & -0.09 & -0.07 & 0.72 \end{pmatrix}$	$\begin{pmatrix} 1.63 & 1.56 & 1.44 & -0.10 & -0.03 & 0.02 \\ 0.79 & 1.25 & 0.99 & 0.08 & -0.04 & 0.07 \\ 1.32 & 1.21 & 1.55 & 0.01 & -0.06 & 0.05 \\ -0.02 & 0.02 & 0.06 & 0.10 & 0.07 & -0.05 \\ -0.03 & -0.15 & -0.04 & -0.09 & 0.27 & -0.06 \\ 0.10 & 0.12 & 0.06 & 0.02 & -0.06 & 0.21 \end{pmatrix}$
C6PN	$\begin{pmatrix} 3.88 & 2.37 & 1.31 & 0.43 & -0.68 & -0.37 \\ 2.58 & 4.48 & 2.69 & 0.07 & -0.57 & 0.30 \\ 3.08 & 3.27 & 4.18 & 0.53 & 0.41 & 0.20 \\ -0.53 & -0.79 & -0.98 & 0.66 & -0.08 & -0.22 \\ -0.31 & 0.00 & 0.25 & 0.00 & 1.32 & 0.00 \\ -0.25 & -0.39 & 0.09 & -0.26 & 0.60 & 0.86 \end{pmatrix}$	$\begin{pmatrix} 1.37 & 0.94 & 0.96 & 0.16 & 0.14 & 0.12 \\ 1.65 & 2.74 & 1.36 & 0.03 & 0.16 & -0.08 \\ 1.20 & 2.07 & 3.05 & -0.21 & 0.13 & -0.18 \\ -0.06 & 0.13 & 0.09 & 0.24 & 0.12 & 0.14 \\ -0.09 & -0.12 & -0.05 & -0.08 & 0.59 & -0.03 \\ 0.15 & 0.09 & 0.12 & -0.11 & -0.14 & 0.09 \end{pmatrix}$	$\begin{pmatrix} 1.63 & 1.56 & 1.44 & -0.10 & -0.03 & 0.02 \\ 0.79 & 1.25 & 0.99 & 0.09 & -0.03 & 0.07 \\ 1.32 & 1.21 & 1.55 & 0.01 & -0.06 & 0.05 \\ -0.02 & 0.12 & 0.06 & 0.10 & 0.06 & -0.05 \\ -0.03 & -0.15 & -0.04 & -0.09 & 0.27 & -0.06 \\ 0.14 & 0.04 & 0.06 & 0.02 & -0.06 & 0.21 \end{pmatrix}$

Table 4
Isotropic elastic constants (in GPa) for PN, C5PN and C6PN at different temperatures

Polymer	T (K)	Tensile modulus	Bulk modulus	Shear modulus	Poisson's ratio
PN	300	1.41	2.68	0.50	0.41
	400	0.28	1.50	0.10	0.47
	500	0.22	1.11	0.07	0.47
C5PN	300	1.56	2.56	0.59	0.40
	400	0.67	1.57	0.24	0.43
	500	0.37	1.31	0.13	0.45
C6PN	300	2.25	3.09	0.81	0.38
	400	1.40	1.71	0.51	0.36
	500	0.69	1.48	0.24	0.42

MSD approaches diffusive behavior above 400 K and therefore the drop in the modulus is more compared to C6PN where the MSD remains very small at all temperatures. In addition, the results for the mechanical properties are also in accord with the slower conformational dynamics observed in the case of C6PN versus C5PN. We note in passing that the trends observed for the bulk and shear moduli follow along similar lines to that seen in the tensile modulus case.

4. Conclusions

The effects of introducing POSS moieties onto polymeric chains as pendant groups have been explored via atomistic molecular dynamics simulations. The simulation predicted volume–temperature properties and X-ray scattering intensities are in good agreement with experimental results for all three polymers studied. An increase in the glass transition temperature is seen upon incorporation of the C5POSS and C6POSS moieties. The T_g for C5POSS containing polynorbornene was predicted to be higher than that for C6POSS. Chain packing around the C5POSS moieties was more efficient compared to that around C6POSS moieties. This was traced to the intrinsic conformational attributes of the moieties arising out of the contrasting behavior of cyclopentyl versus cyclohexyl rings attached to the POSS polyhedra. Cyclopentyl groups pack more efficiently around the POSS moieties (can approach the polyheral cage composed of Si and O atoms more closely) compared to cyclohexyl groups that tend to fan out being subject to large steric hindrances. The mobility of the POSS moieties in the polymer was addressed via the mean squared displacements. In both cases the MSD was very small, with that for C6POSS being smaller compared to C5POSS. Conformational dynamics were also retarded by the presence of the POSS moieties as ascertained via the computation of the torsional autocorrelation function. It was demonstrated that the main chain dynamics was sensitive not only to the presence but also to the nature of the POSS moieties attached to it. Chain dynamics was slower in the case of the polymer with C6POSS pendant groups compared to that with C5POSS pendant groups. These results are in good agreement with the mechanical properties predicted from simulations where the tensile, bulk and shear moduli for C5PN and C6PN copolymers show an increase and change less dramatically with increasing temperature compared to the polynorbornene homopolymer. No evidence for intermolecular aggregation was seen from the packing analysis. However, it is not implied that aggregation cannot occur since the temporal and spatial scales employed in the atomistic level simulations here do not permit such a determination. Rather it is demonstrated that in the case where no aggregation is present, the beneficial effects of incorporating the POSS moieties are realized nevertheless. The source of the reinforcement is therefore traced to the ponderous nature of the POSS moieties that behave as strong anchoring points in the polymeric matrix rather than any specific intermolecular interactions between the POSS moieties.

Acknowledgements

We are indebted to the Materials and Manufacturing Directorate at the Air Force Research Laboratory, Wright Patterson Air Force Base, for financial support of this work. We extend our appreciation to W.W. Adams, A.V. Fratini, J.D. Lichtenhan, P.T. Mather and S.J. Phillips for their interest and encouragement in this endeavor. Most of the computations were carried out at the Major Shared Resource Center of the Aeronautical Systems Center (ASC/MSRC). We gratefully acknowledge the assistance of J. Henes (University of Dayton Research Institute) for managing the computational facilities and Nazy Khosrovani (Molecular Simulations Incorporated) for her assistance with the MSI software.

References

[1] Lichtenhan JD. Commun Inorg Chem 1995;17:115.
[2] Schwab JJ, Haddad TS, Lichtenhan JD, Mather PT, Chaffee KP. Antec 1997;611:1817.
[3] Shockey EG, Bolf AG, Jones PF, Schwab JJ, Chaffee KP, Haddad TS, Lichtenhan JD. Appl Org Chem 1999;13:311.

[4] Mather PT, Jeon HG, Romo-Uribe A, Haddad TS, Lichtenhan JD. Macromolecules 1999;32:1194.
[5] Haddad TS, Lichtenhan JD. Macromolecules 1996;29:7302.
[6] Romo-Uribe A, Mather PT, Haddad TS, Lichtenhan JD. J Polym Sci, Part B: Polym Phys 1998;36:1857.
[7] Lichtenhan JD, Otonari YA, Carr MJ. Macromolecules 1995;28:8435.
[8] Tschucida A, Bolln C, Sernetz F, Frey H, Mulhaupt R. Macromolecules 1997;30:2818.
[9] Lichtenhan JD, Vu NQ, Cater JA, Gilman JW, Feher F. Macromolecules 1993;26:2141.
[10] Mantz RA, Jones PF, Chaffee KP, Lichtenhan JD, Gilman JW, Ismail IMK, Burmeister MJ. Chem Mater 1996;8:1250.
[11] Lee A, Lichtenhan JD. Macromolecules 1998;31:4970.
[12] Hong B, Thoms TPS, Murfee HJ, Lebrun MJ. Inorg Chem 1997;36: 6146.
[13] Zhang C, Babonneau F, Bonhomme C, Laine RM, Soles CL, Hristov HA, Yee AF. J Am Chem Soc 1998;120:8380.
[14] InsightII 4.0.0P San Diego, CA: Molecular Simulations Inc., 1999.
[15] Andersen HC. J Chem Phys 1980;72:2384.
[16] Berendsen HJC, Potsma JPM, van Gunsteren WF, DiNola A, Haak JR. J Chem Phys 1984;81:3684.
[17] Swope WC, Andersen HC, Berens PH, Wilson KR. J Chem Phys 1982;76:637.
[18] Verlet L. Phys Rev 1967;159:98.
[19] Rutledge GC, Suter UW. Macromolecules 1991;24:1921.
[20] Allen MP, Tildesley DJ. Computer simulation of liquids. Oxford: Oxford University Press, 1987.
[21] Boyd RH. Trends Polym Sci 1996;4:12.
[22] Han J, Gee RH, Boyd RH. Macromolecules 1994;27:7781.
[23] Bondar VI, Kukharskii YM, Yampolskii YP, Finkelshtein ES, Makovetskii KL. J Polym Sci, Part B: Polym Phys 1993;31:1273.
[24] Yampolskii YP, Finkelshtein ES, Makovetskii KL, Ostrovskaya IY, Portnykh EB, Gringolts ML, Ishunina YG, Kevdina IB, Shantarovich VP. Vysokomol Soedin 1996;38:1480.
[25] Pant PVK, Han J, Smith GD, Boyd RH. J Chem Phys 1993;99:597.
[26] Takeuchi H, Okazaki K. J Chem Phys 1990;92:5643.
[27] Kohlrausch R. Pog Ann 1847;12:393.
[28] Williams G, Watts DC. Trans Faraday Soc 1970;66:80.
[29] Williams G, Watts DC, Dev SB, North A. Trans Faraday Soc 1971; 67:1323.
[30] Leipholz HHE. Theory of elasticity. Leyden: Noordhoff, 1974.
[31] Parinello M, Rahman A. J Chem Phys 1982;76:2662.
[32] Gusev AA, Zehnder MM, Suter UW. Phys Rev B 1996;54:1.
[33] Zehnder MM, Gusev AA, Suter UW. Revue De L'Institut Francais Du Petrole 1996;51:131.
[34] Gusev AA, Zehnder MM, Suter UW. Macromolecules 1994;27:615.
[35] Parinello M, Rahman A. Phys Rev Lett 1980;45:1196.